Mining of Mineral Deposits
Volume 19 (2025), Issue 3, 1-13

MMD JOURNAL / MINING.IN.UA

https://doi.org/10.33271/mining19.03.001

Longwall mining-induced weighting mechanism and its interactions with shield support and coal wall

Tien Dung Le [1,2*], Cao Khai Nguyen [1,2], Manh Tien Tran [1,2]

[1] *Hanoi University of Mining and Geology, Hanoi, Vietnam*
[2] *Research Group: Sustainable Development of Mining Science, Technology and Environment, Hanoi University of Mining and Geology, Hanoi, Vietnam*

**Corresponding author: e-mail t.d.le@humg.edu.vn*

Abstract

Purpose. Rock mass surrounding an underground space, especially in the case of longwall mining, may experience severe instabilities if the overburden facilitates a weighting event. This paper presents a detailed study of the longwall mining-induced weighting mechanism and its interactions with shield support and coal wall.

Methods. Using the real-time monitoring data of shield and geological-mining conditions, this paper develops a panel-scale DEM model of longwall retreat to understand the mechanism of mining-induced weighting better.

Findings. The study clearly details the profiles of horizontal and vertical stresses in the main roof strata. During periodic weighting, a re-concentration of horizontal stress at the clamped end of the cantilever roof beam is demonstrated, reaching a peak of 1.5 times the pre-mining value. Apart from the primary breaking at the clamped end, a cantilever roof beam may experience a secondary breaking near its middle. Within the main roof, the intact rocks were found to fail in tension, while the geological structures mostly failed in shear.

Originality. The study reveals that while an increase in shield stiffness and yield force delays the occurrence of the weighting event, the associated longer span of voussoir/cantilever roof beams increases the coal block detachment at the wall. In contrast, an increase in the set-to-yield ratio of the shield shortens the weighting intervals, and this accordingly decreases the coal wall detachment. For coal seams, stiffer coal and stronger coal delay the occurrence of weighting. The stiffer coal, meanwhile, clearly improves coal wall stability despite the negative impact from the greater weighting interval. A faster longwall retreat rate also improves coal wall stability while delaying the occurrence of weighting.

Practical implications. The findings of this paper assist engineers in better identification and response to geotechnical hazards in underground space, maintaining a safe workplace, and minimising environmental impact.

Keywords: *underground mining, roof weighting, rock beam failure, real-time monitoring, shield design, coal wall stability*

1. Introduction

Longwall mining contributes a significant part to underground coal extraction worldwide. While the longwall mining beneath easy-to-cave roof has proven its high efficiency and safety, the mining beneath hard-to-cave roof, a condition not uncommon in coal industries where large coal reserves exist, may result in critical geomechanical incidents such as a weighting event. A weighting event commonly refers to the maximum concentration and relief of roof pressure associated with breaking roof strata that do not cave right after shield support advance (Fig. 1). An event can be formed when near-seam (e.g., no greater than 70 m [1]) and thickly bedded strong strata (e.g., greater than 2 m [2]) overhang above mined-out area (goaf), significantly increasing load on shield support and coal wall before failing, breaking and relieving abutment stress. In severe cases, a weighting is commonly accompanied by coal wall spalling, roof cavity, shield damage, and even coal burst, windblast or massive longwall collapse [3].

Longwall mining-induced weighting with significant strata disturbance causes unsafe workplace and production stoppage and long-term environmental impacts such as loss of non-renewable resources, change of regional underground water bodies and surface plants, and emission of greenhouse gases. A thorough insight into the weighting's geomechanical mechanism and its interactions with shield support and coal wall is critically important to minimise the event's occurrence and impact, from which safer and more environmentally sustainable underground mining can be achieved.

Extensive mining practice and analytical failure models revealed that the first weighting (also known as initial weighting or main weighting) can be explained by the occurrence and failure of the voussoir roof beam [4]-[8]. However, the periodic weighting after the first weighting is associated with the periodic breaking of the cantilever roof beam or the detachment of a large roof block. Further detailed mechanisms of the weighting formation can be found in previous numerical and physical modelling studies.

Received: 10 January 2025. Accepted: 13 May 2025. Available online: 30 September 2025

Mining of Mineral Deposits. ISSN 2415-3443 (Online) | ISSN 2415-3435 (Print)

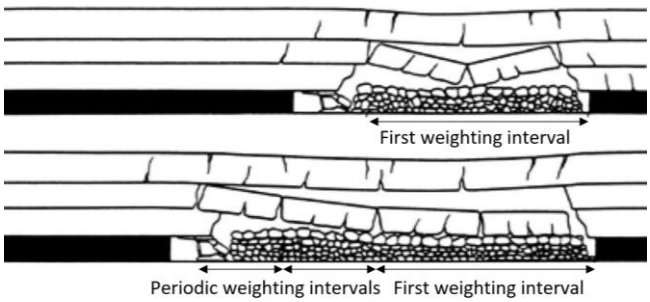

Figure 1. Illustration of longwall mining-induced weighting (modified from [4])

For example, by performing Discrete Element Method (DEM) modelling, Shabanimashcool, Jing [9] suggested that during the first weighting, the voussoir beam is formed in jointed roof strata and reaches a maximum deflection of 70% of the stratum thickness before strata caving.

Using a similar modelling method, Le et al. [10] visually demonstrated the concentration of horizontal stress associated with first weighting and stated that the voussoir beam fails in crushing mode. Through numerical and physical modelling, Kang et al. [11] found that the voussoir beam predominantly fails in snap-through mode. They further stated that an increase in horizontal stress up to five times the pre-mining value is a threshold for the precursor of massive roof collapse. Developing a meshless numerical modelling method, Zhou et al. [12] confirmed the strong correlation between roof weighting and roof collapse, and the collapsed roof forms a trapezoid shape. After the first weighting, the periodic weighting was stated to involve both shear and tensile fractures and overburden convergence [13]. The rock failure is initiated in the upper section of the cantilevering strata and progresses downwards into the coal seam. Along with the local roofs composed of cantilever beams, Gao et al. [14] proved that the periodic weighting also involves the rupture of the upper strata bridge. The above studies provided detailed insight into the weighting mechanism. Still, unfortunately, the critical role of coal wall and shield support in the weighting occurrence was either not explicitly considered or sufficiently interpreted. The limitation in representing natural coal fracturing and/or real shield behaviour in those studies is a possible reason.

Apart from the occurrence mechanism, the interactions among roof weighting, shield support and coal wall have been studied in the literature. For interaction between roof weighting and coal wall, Behera et al. [15] stated that the first weighting causes 53% of the coal wall length to experience excessive wall spalling with a depth of 3 m. Murmu and Budi [16] found that the first weighting consists of two distinct phases of peak stress and main fall, and this event leads to a maximum extent of 2 m coal wall spalling. While Wang et al. [17] confirmed that the brittle rupture of main roof results in dynamic load on coal wall, Le et al. [10] further found that this rupture affects the caving of top coal behind shield support. The reader is referred to Le and Bui for the impact of coal stiffness and strength on the roof's first weighting [18]. Khanal et al. [19] demonstrated that massive strata result in higher chock convergence than bedded strata for interaction between weighting and shield support. Greater chock convergence occurs when the chock is left standing longer. The authors also stated that in adverse conditions such as strong and hard-to-cave sandstone channels, a chock capacity of greater than 800 tons may be required [20]. Singh and Singh [21] demonstrated that greater shield capacity reduces roof convergence, but this may not be true in deep mining. They also noted that installing stiffer support may lead to unnecessary loading in deep mining. Wang, Li [22] confirmed that the controlling effect of shield to coal wall is strongest when its stiffness is in the range of 1-100 MN/m, and roof pressure transferred to coal wall is negatively related to support stiffness. While the above studies contributed to interpreting the interaction between roof weighting and coal wall or between the weighting and shield, the interactions among all three objectives at the same time appear to be little analysed. Because roof weighting, shield support and coal wall simultaneously interact as is the practice case, this should be considered for a more reliable insight into the weighting mechanism.

This paper presents a detailed study of the longwall mining-induced weighting mechanism and its interactions with shield support and coal wall. The occurrence of first and subsequent events is analysed using panel-scale numerical modelling of a typical longwall mining experience roof weighting. The longwall model is verified against the field's real-time monitoring data of shield support. The interactions among weighting events, shield support and coal wall are studied through parametric studies of shield and coal characteristics. The findings of this paper help engineers better identify and respond to geotechnical hazards in underground space, maintain a safe workplace, and minimize environmental impact and resource loss.

2. Mine A and real-time shield data

2.1. Mine A conditions and weighting event

Mine A is located in northeast Australia (Fig. 2), where its longwall mining has experienced weighting events. The mine extracts a 90-330 m deep coal seam (Goonyella Middle Seam – GMS) with an average thickness of 5.5-7.5 m and a dip angle of three degrees [7].

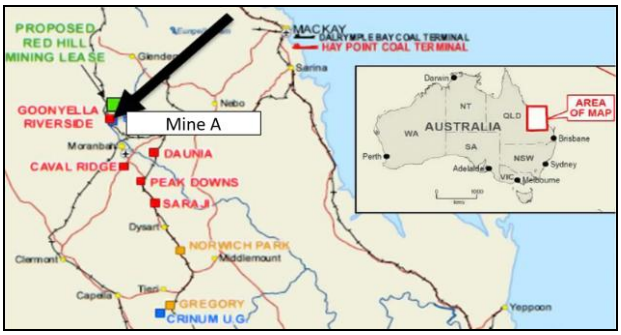

Figure 2. Location of Mine A in Australia (modified from [7])

A thin siltstone immediate roof overlies the seam up to 6 m thick, a thick sandstone main roof up to 40 m (MP42 sandstone), and upper thick siltstone strata interbedded with thin coal seams and thin sandstone bands (Fig. 3).

While the immediate roof is thinly bedded and weak, the main roof is moderately and relatively strong up to 40-60 MPa. At the coal basin scale, the joints predominantly strike east-west with a deviation of 10-20 degrees [23]. The joints' spacing is proportional to their height and increases from coal seam to siltstone and sandstone.

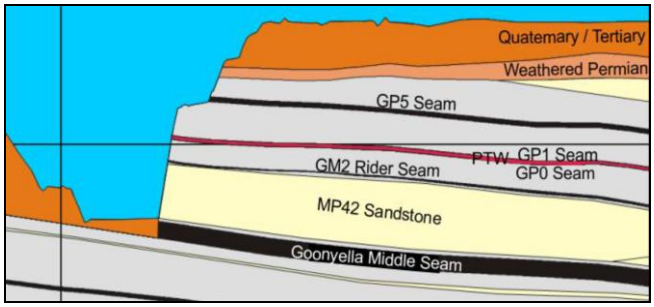

Figure 3. Cross-section view at high wall exposure of Mine A (modified from [7])

At the mine scale, in-seam fractures appear to form a discrete fracture network with more or less vertical orientation. The maximum horizontal stress predominantly orientates north-northeast to south-southwest and is 1.6-2.7 times the vertical stress [24], [25]. Mine A designs longwall panels in east-west direction, and the first weighting typically occurs after 60-70 m of longwall retreat [7]. The shield in panels has two legs, 2 m in width, and a maximum capacity of 1460 tons.

2.2. Analysis of real-time shield data

The mine operators monitored the Time-Weighted Average Pressure (TWAP) and averaged leg pressure in real time. The first pressure was a key indicator of weighting event [4], while the second was used to profile shield leg force during longwall retreat. The TWAP data for the current analysis were from the start to the next two months of a typical longwall mining, corresponding to about 250 m longwall retreat (Fig. 4).

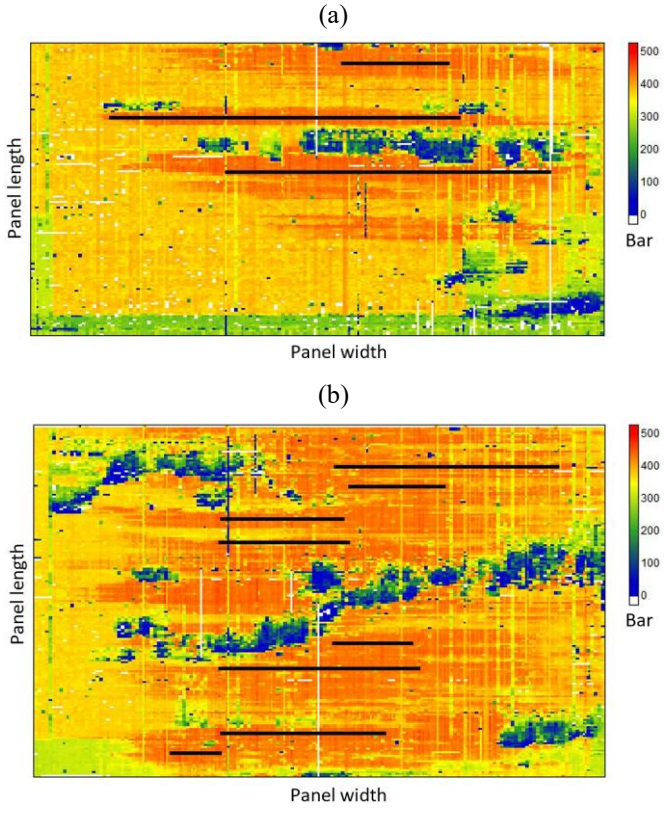

Figure 4. Time-Weighted Average Pressure map in (a) the first 30 days (data from Le, Oh [10]) and (b) the next 30 days of a longwall retreat at Mine A

It should be mentioned that although the original data for generating the TWAP map in Figure 4a was used in [10], the TWAP value determining a weighting event was too low in the mentioned study. This resulted in a greater number and shorter interval of weighting events than those in practice [7]. In the current study, by considering a TWAP value of greater than 430 bar (equivalent to a shield leg force of 6.84 MN) for determining a weighting, Figure 4a shows that in the first 30 days (110 m of retreat), the first weighting occurred at 61 m of retreat and spanned over Shield 54 to Shield 144 along panel width. The second weighting occurred at 79 m of retreat and spanned over Shields 22-119. The third weighting occurred at 102 m of retreat and spanned over Shields 86-116. In the first 30 days of longwall retreat, there were three weighting events that mainly occurred at the mid-panel width and spanned over at least 30 shields in this direction. In the next 30 days of operation (142 m of retreat), Figure 4b shows a weighting interval ranging from 6 to 17 m in panel strike and a shorter panel width span than in the first period. The weighting number and interval identified from the current study agree well with those in Coutts, Lynch [7].

Figure 5 shows the profile of the averaged leg force of Shield 90 – the shield experienced major weighting events and was at the mid-panel width during longwall retreat.

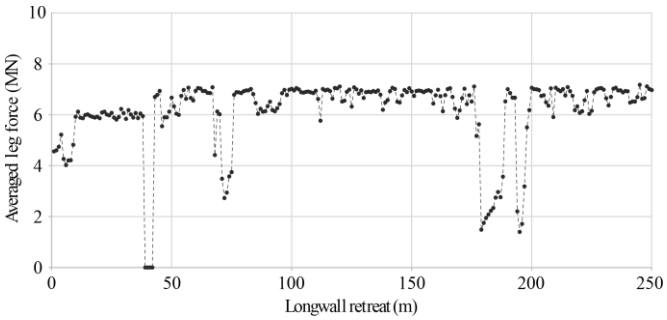

Figure 5. Averaged leg force of Shield 90

The figure shows that from the start of the retreat, the leg force markedly increased in the first four meters before rapidly decreasing in the next four meters. This increase and decrease force cycle can be attributed to the start and completion of the first caving of the top coal section. In practice, the caving was completed in 8-10 m of retreat as stated in Le, Oh [10]. The force then significantly increased to a peak value when the longwall retreated 11 m before decreasing to a low value at 20 m of the retreat. The second increase and decrease cycle of leg force was likely associated with the first caving of the immediate roof strata. In the following longwall retreats, the leg force steadily fluctuated during the periodic caving of top coal and the immediate roof. As the longwall retreated further, the force followed significant increase and decrease cycles. These cycles were related to the increasing deflection of the main roof strata and the breaking of the lowest strata layers. When the longwall retreated 61 m from its start, the leg force reached a peak value of 7.05 MN and remained high (6.84-7.08 MN) in the next 6 m before rapidly decreasing to a low value (2.73 MN) at 72 m of total retreat. This increase and decrease cycle indicated the first weighting of the main roof (Fig. 4), which lasted during 6 m of retreat. Similarly, the subsequent cycles of leg force occurred at 73-86 and 87-112 m of retreat, clearly reflecting the second and third weighting events,

respectively. In Figure 5, some cycles were unrelated to weighting events, and zero force reflected the missing data. The real-time monitoring of Shield 90 also revealed that the leg closure was greatest during the first weighting (maximum of 400 mm) and lower during periodic events (maximum of 200 mm).

3. Modelling of longwall mining-induced weighting

3.1. Modelling of longwall considering roof weighting

The DEM-based numerical program UDEC [26] was used to model longwall mining by considering roof weighting. The program is particularly suitable for analysis of rock mass failure caused by large-scale underground excavation because it can well represent the internal stress, external load, different failure modes and small deformation to complete detachment associated with rock mass within a finite period. The reader is referred to the program's manual for detailed theory and example applications in rock mechanics. Due to the two-dimensional plane-strain formation of the program, the longwall mining was modelled along the chainage of Shield 90, where initial and periodic weighting events occurred as analysed earlier. A complete geometry of the longwall mining model was constructed in Figure 6 with detailed justification.

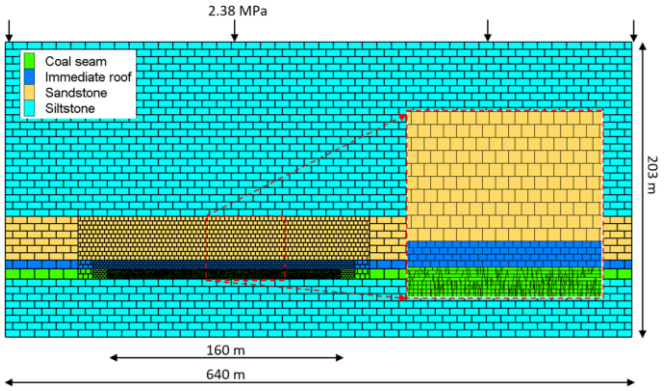

Figure 6. Longwall mining model considering roof weighting

Along the model width, the longwall retreat length should be sufficient for at least 2-3 weighting events to be formed. Based on the weighting analysis from Shield 90 (Section 2.2), the retreat length was selected to be 160 m, including an 8 m wide installation room. The total model width was accordingly 640 m, being four times the retreat length. Along the model height, a 7, 6, and 30 m thickness was assigned to the coal seam (GMS), immediate roof, and main roof (MP42), respectively. Below and above these areas of interest, the strata thickness was selected to be 40 and 120 m to minimise the impact from the bottom and top boundaries on these areas, respectively. Since the on-site mining started below an average cover depth of 260 m, the remaining thickness of overburden (97 m) was implicitly modelled by a compressive stress on the top boundary (2.38 MPa). The model height was accordingly 203 m in total.

Inside the areas of interest, a bedding spacing of 0.8-0.95, 1.5, and 3 m was assigned to coal seam, immediate roof and main roof, respectively, due to the sedimentary nature of coal-measure rocks. The spacing was up to 5 m around the areas of interest. Vertical joints were assigned to non-coal areas with 1-3 times the bedding spacing in the exact location for model simplification. In coal seams, the in-seam fractures should be modelled as realistically as possible to facilitate the response of the coal wall to roof weighting. Based on the geological conditions in Section 2.1, the fractures were modelled as a discrete fracture network using the DFN module in UDEC. The reader is referred to the program's manual for a fundamental description and use of the module [26]. The fractures' orientation followed a Gaussian distribution with a mean dip angle of 90 degrees and a standard deviation of 10 degrees. The fracture size and position were assumed to follow a uniform distribution without field data. The mass density for stopping fracture generation was estimated to be 0.8 m/m^2, which should induce top coal to cave in a 0.2-1 m block diameter as observed in the field. The final realisation of the in-seam fractures was selected so that the cyclic caving of top coal occurred right after each shield support advance.

The strain-softening law was assigned to blocks in the areas of interest to model rock mass behavior to facilitate pre- and post-failure behaviours. The Mohr-Coulomb law was applied to blocks outside the areas of interest due to incomplete block/layer detachment. Input properties for the laws were derived from published laboratory tests at Mine A and neighbouring mines, empirical factors scaling rock properties from laboratory to field scale, and modelling experience from relevant studies. For example, coal's Uniaxial Compressive Strength (UCS) was 11.7 MPa, falling within the range tested in Seedsman [27]. The UCS of immediate, siltstone, and sandstone rocks was 22, 29, and 44 MPa, as reported by Clarkson [28]. These laboratory UCS values were scaled to field values using a reduction factor 0.5 based on the typical rock size in model [5]. The elastic modulus was 2.2 GPa for coal and 200 times the UCS (MPa) for other rocks. The moduli were scaled for modelling using a factor of 0.469, as recommended by past numerical studies [29]. The Poisson's ratio was 0.25 for all rocks due to sedimentary formation. The post-failure strength reduction and critical strain were adopted from Shen and Duan [30]. For geological structures, the Coulomb slip law was assigned. The structure's stiffness was derived from a trial-and-error process, referring to the shear stiffness range of 1-3 GPa/m published in past studies [31], [32]. The structures' friction was lowest in the coal seam and immediate strata, while it was greater in the siltstone and sandstone strata. The structures' cohesive and tensile strengths were assumed to be zero and very low in the field. The rock material properties used in the longwall mining model are summarised in Table 1.

For the model equilibrium before mining, the side and bottom boundaries were fixed. The top boundary was assigned compressive stress, as mentioned earlier. In-situ stress was assigned explicitly to the coal seam, floor strata and roof strata due to different rock densities and strata thicknesses. The horizontal stress was twice the vertical stress in all strata.

3.2. Longwall retreat cycle and model verification

One longwall retreat cycle was modelled by cutting a 1 m thick coal wall, advancing the shield support to the new coal wall position, running the model to the equilibrium state, and clearing any coal/rock blocks falling onto the recovery space behind the shield. The web cutting and coal/rock clearance were performed by deleting blocks from the model. The shield was modelled by parallel spring elements vertically connecting floor blocks with roof blocks.

Table 1. Rock material properties used in the longwall mining model

Strata	Rock materials									Geological structures		
	Density (kg/m^3)	Uniaxial compressive strength (MPa)	Field elastic modulus (GPa)	Poisson's ratio	Cohesion (MPa)	Tensile strength (MPa)	Residual cohesion (MPa)	Residual tensile strength (MPa)	Critical strain (%)	Standard stiffness (GPa/m)	Shear stiffness (GPa/m)	Friction (degree)
Sandstone	2500	22.00	4.13	0.25	6.65	2.20	1.33	0.22	0.1	50	5	35
Siltstone	2500	14.50	2.72	0.25	4.56	1.45	0.91	0.15	0.1	50	5	25
Immediate roof	2500	11.00	2.06	0.25	3.46	1.10	0.69	0.11	0.1	50	5	15
Coal seam	1500	5.85	1.03	0.25	1.69	0.59	0.34	0.06	0.5	50	5	15

The spacing between two adjacent elements was sufficiently small to avoid block caving inside. Because the default support width in the out-of-plane direction is 1 m in UDEC, the setting and yield forces were modelled as 5.09 and 7.16 MN, respectively. The troops were protected by a 5.3 m-long and 1 m-wide shield in the field. The troops, interestingly, equaled the values generated by one shield leg. The behaviour of the shield element was controlled by an axial force-displacement relationship, as defined in Figure 7.

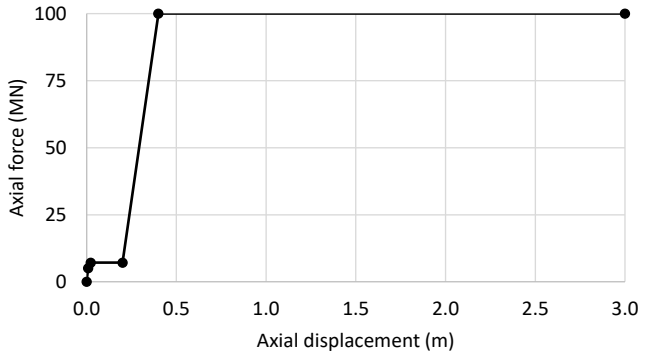

Figure 7. Force-displacement relationship of the shield in the model

The axial displacements for activation of the setting force and yield force were derived from the ground reaction curve at the field [33] and the leg closure analysed in Section 2.2. An incredible force of 100 MN was set at 400 mm of element displacement to avoid excessive shield deformation during the weighing event. The shield advance was modelled by deleting the shield at the previous coal wall, running the model without the shield in a limited timesteps, and setting the shield at the new coal wall.

The weighting mechanism and its interaction with shield support and coal wall were analysed through the main roof's stress, failure, and breaking, the force exerted by shield support, and block detachment at the coal wall during longwall retreat modelling. Within the main roof, separate rates of zone and contact failures were defined by dividing the number of zones/contacts failed when mining to mid-retreat length by the total number of zones/contacts within the area of interest. Similar rates for coal seam were also defined, but for the extent ahead of the coal wall. The shield force was the total force of all elements for shield support. For the coal wall, the number of blocks detached from the coal wall and its roof was counted, representing coal wall spalling and roof cavity. Several new functions were programmed to monitor rates and count block detachment. For roof weighting, an event was identified through shield force (great force followed by significant drop) and roof displacement (significant sagging or breaking) for two reasons: (*i*) yield valve was not modelled due to program limitation and (*ii*) force was recorded at the end of each retreat cycle rather than time-weighted average value.

The model was verified after completing all longwall retreat cycles. The modelled shield force and roof weighting events, as shown in Figure 8, were compared with those in practice (Section 2.2).

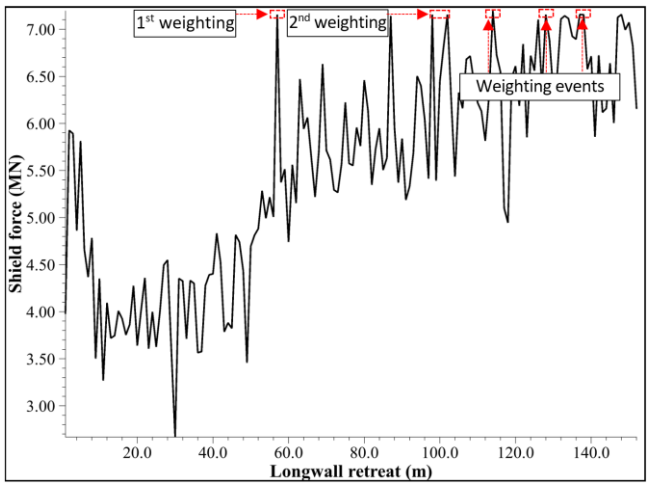

Figure 8. The force exerted by a shield in the model

The figure shows that apart from the first 11 m of retreat, where the modelled force was suddenly high before rapidly dropping due to the creation of the installation room, the modelled force followed a trend and magnitude similar to those at the field. As analysed in Section 4, the first weighting occurred at 57 m of retreat, which was only four meters less than that at Mine A's longwall. Although the second weighting occurred 41 m after the first event, the interval for subsequent events ranged from 9 to 14 m, falling within the 6-17 m range as analysed in Section 2.2.

4. Longwall mining-induced weighting mechanism

4.1. Mining-induced stress and strata failure

The stress tensor induced by longwall mining after every 30 m of retreat is shown in Figure 9. Figure 9a indicates that the stress tensor was uniformly distributed before mining. Because the compressive stress was negative in modelling, the minor principal stress was vertical, while the primary and intermediate principal stresses were horizontal and equal. At 30 m of longwall retreat, the stress was significantly relieved from the goaf and transferred to the surrounding rocks (Fig. 9b).

This simultaneously formed the stress relief zone covering the goaf and the stress concentration zone ahead of the coal wall. The minor principal stress was relieved in the main roof and immediate floor within the relief zone, but the major principal stress still existed in the unbroken strata.

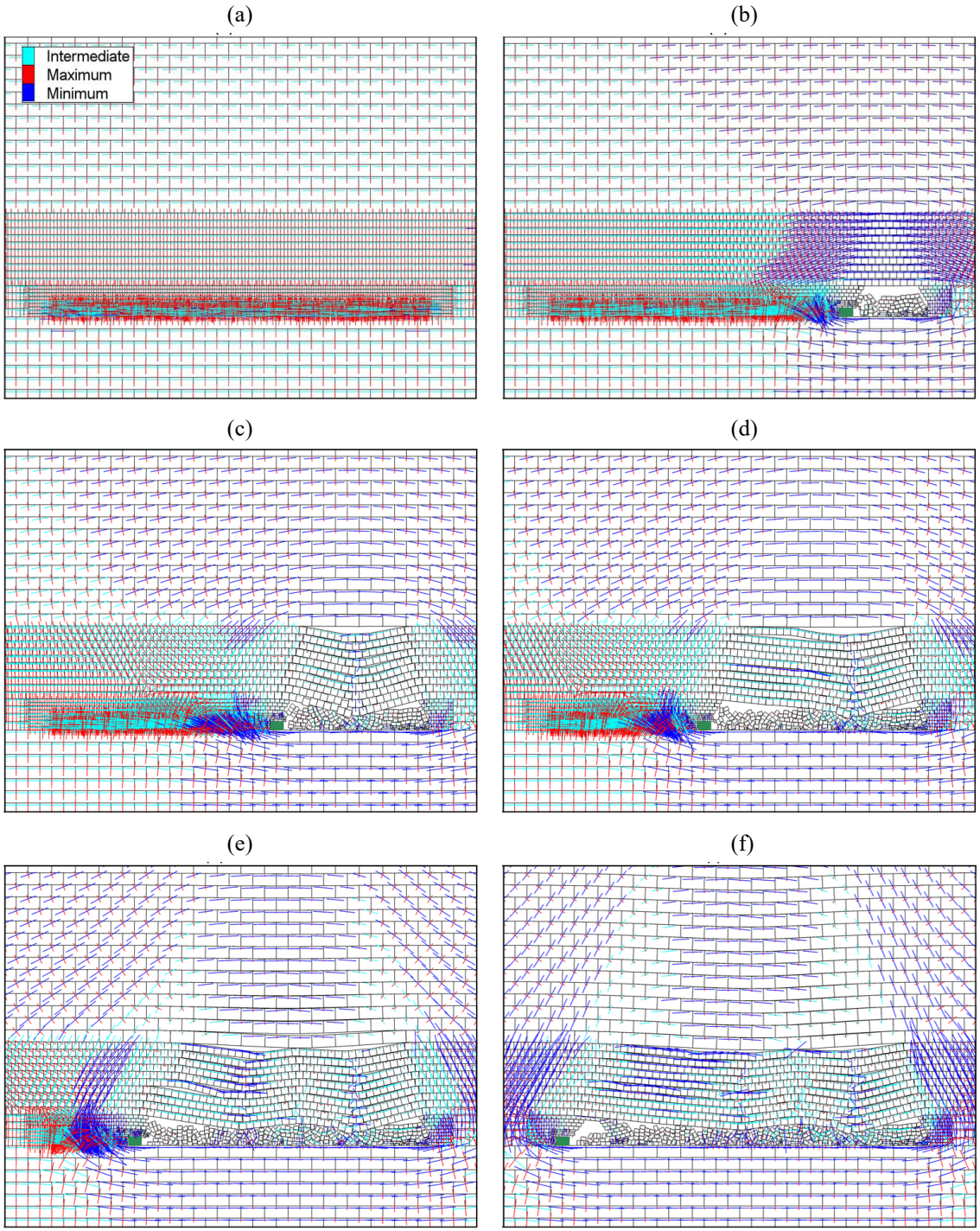

Figure 9. Stress tensor at a mining interval of 30 m: (a) 0 m; (b) 30 m; (c) 60 m; (d) 90 m; (e) 20 m; (f) 150 m

At 60 m of retreat, the main roof strata failed and broke beforehand (Fig. 9c). The stress was accordingly relieved from the main roof, which expanded the stress relief zones and concentration. As the longwall retreated further, the stress relief and concentration zones continued to grow (Fig. 9d). The zones reached a limited extent when the roof strata reached a steady-state movement (Fig. 9e-f).

Along with the formation of stress relief and concentration zones, Figure 9 illustrates the change in stress orientation and magnitude around the relief zone. For example, the major principal stress shifted from horizontal before mining to vertical ahead of the coal wall and inclined in the main roof and floor strata. The orientation and magnitude, however, gradually recovered their pre-mining state at areas far away from the relief zone. The mining-induced stress characteristics in the current study agree well with those in previous studies [4], contributing to the model verification.

The detailed stress change within the main roof strata is analysed from Figure 10. The figure depicts vertical and horizontal stresses along the mid-MP42 height, 28 m above the seam floor. Before the mining, vertical and horizontal stresses were 5.75 and 11.5 MPa, respectively (Fig. 10a).

At 30 m of retreat and before the first breaking of the main roof, the vertical stress significantly dropped to a low value within the interval vertically above the goaf area. At the same time, this stress increased to 7 MPa both ahead of and behind such an interval (Fig. 10b).

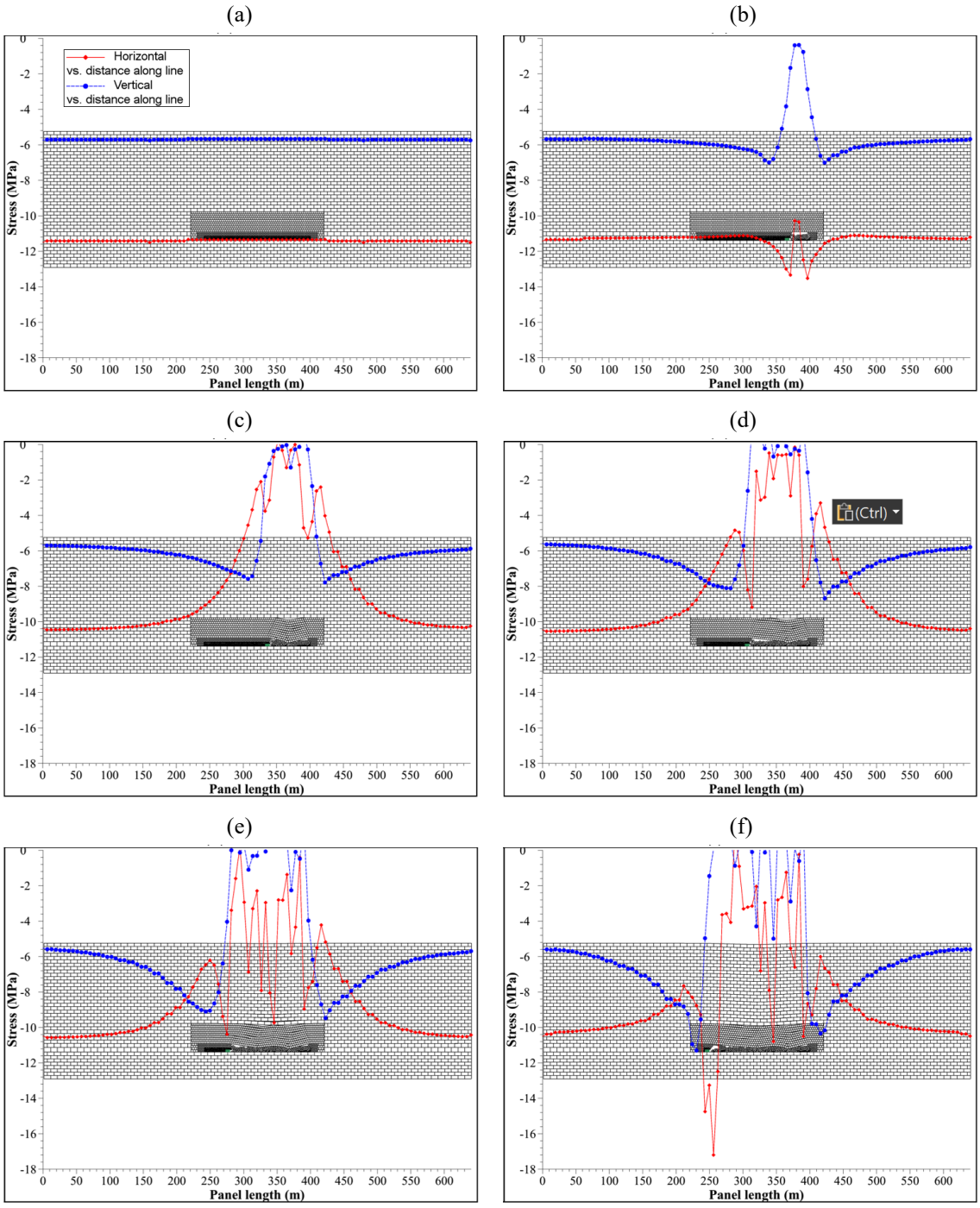

Figure 10. Stress along mid-MP42 height at a mining interval of 30 m: (a) 0 m; (b) 30 m; (c) 60 m; (d) 90 m; (e) 120 m; (f) 150 m

Similarly, the horizontal stress slightly decreased to 10.3 MPa within the interval vertically above the goaf, while it increased to 13.5 MPa at the two sides of the interval. These changes in stress reflected the significant relief of vertical stress due to the underlying strata caving and coal extraction and concentration of horizontal stress in the hanging roof strata (Section 4.2 for a detailed explanation of stress concentration). At 60 m of retreat, the vertical stress continued to increase at the sides of the interval vertically above the goaf (Fig. 10c). The horizontal stress was, however, significantly relieved within the interval because the main roof broke beforehand. As the longwall retreated further to the panel end, the vertical stress continued its trend of change with a peak abutment being two times the pre-mining stress ahead of coal wall (Fig. 10f). The horizontal stress, while being relieved throughout the area of interest, sharply re-concentrated at the area vertically above coal wall. This concentrated stress reached a peak value of 17.3 MPa, being 1.5 times the pre-mining stress (Fig. 10f). The re-concentration was attributed to the failure and breaking of upper strata, which relieved and transferred the horizontal stress from upper strata to main roof below and bending effect of the cantilever roof beam about the wall (Section 4.2).

Also, the horizontal stress could re-concentrate in the broken main roof due to rock reconsolidation. In Figure 10f, the peak horizontal stress occurred vertically above the coal wall, which can be considered the clamped end of a cantilever beam. As visually observed from Figure 10d-f, the location of peak horizontal stress was closer to the goaf than that of peak vertical stress.

The strata failure at 30 m (before first breaking of main roof), 75 m (at mid-retreat length and after first breaking of main roof) and 130 m (failure range still within area of interest) of longwall retreat is shown in Figure 11.

Two modes of material failure (shear/slip and tension) were displayed for intact rocks (via finite-difference zones composing deformable blocks) and geological structures (via contacts between blocks). For the extent of strata failure, the figure shows that as the mining progressed, the extent of failure of intact rocks and geological structures increased. For example, the extent of failed rocks was mostly within coal seam and immediate roof, which was up to 7 m away from coal wall at 30 m of retreat (Fig. 11a). This extent increased to upper strata above main roof and at 17 m ahead of coal wall at 130 m of retreat (Fig. 11c). At the same time, the extent of failed structures also increased to more above main roof and further away from coal wall. The increase in the extent of strata failure during mining is consistent with that in the literature [14].

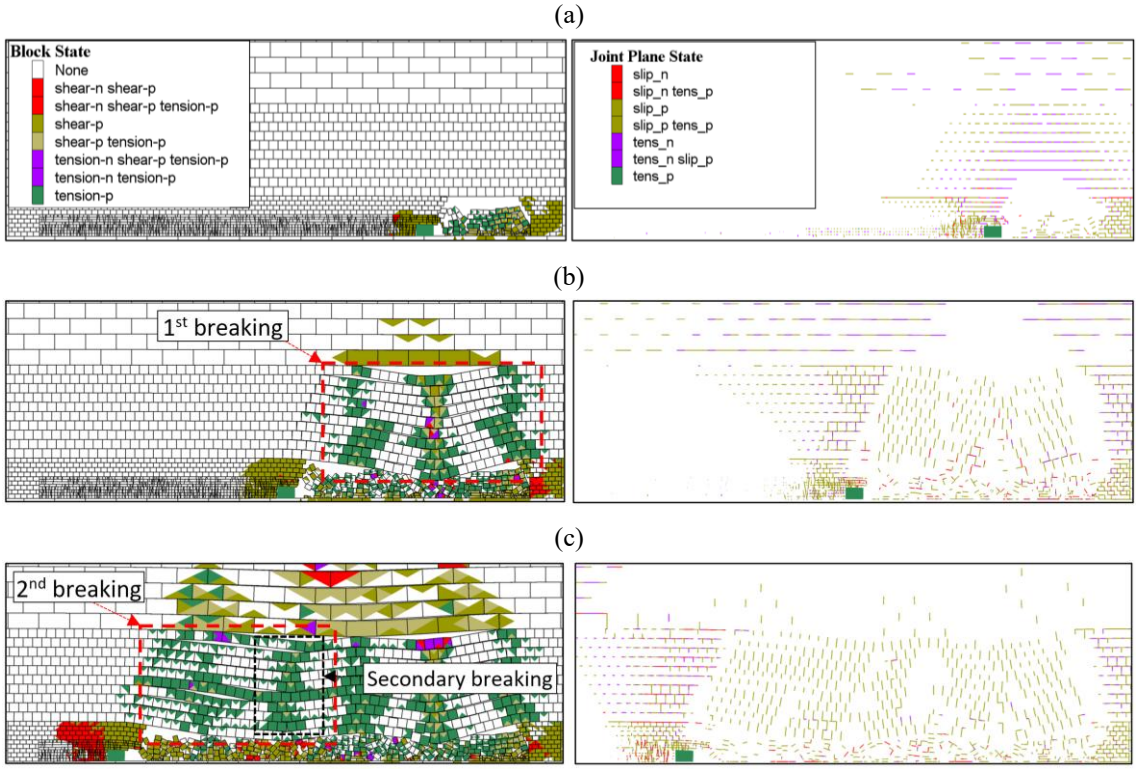

Figure 11. Extent and mode of strata failure of longwall retreat at this distance: (a) 30 m; (b) 75 m; (c) 130 m

The monitoring at the mid-retreat length shows that the coal seam and the immediate roof mostly failed in shear (Fig. 11b). In the coal seam, zone and contact failure rates in shear were 8.53 and 8.38%, respectively. The rates were greater than those failed in tension, which were only 0.02% for the zone and 1.77% for the contact, respectively. The predominant shear failure was attributed to the inability of low shear strength coal within the stress concentration zone. Main roof rocks, however, mostly failed in tension (27.14%) rather than shear (4.71%). The predominant tensile failure in the main roof was associated with the strata weighting and breaking, as analysed in Section 4.2. Also, in the main roof, the geological structures failed in shear and tension with a rate of 44.03 and 14.39%, respectively. The separation of roof layers mainly caused the non-negligible tension failure.

4.2. Mechanism of first and periodic weighting

The first weighting of roof strata was found to occur at 57 m of retreat modelling, which was associated with the first breaking of the main roof strata. The formation mechanism of the event can be analysed from the retreat immediately before breaking, which was at 56 m from the longwall start (Fig. 12). Compared to Figures 9, 10 and 12a clearly shows the concentration of horizontal stress at the middle and two sides of the hanging roof strata. In the middle, the horizontal stress concentrated in the upper portion of each rock layer, reaching a peak of 18.68 MPa, which was 1.62 times the pre-mining stress. The horizontal stress, however, decreased in the lower portion of the layer, which was less than 5 MPa and about half of the pre-mining stress. Figure 12b indicates that because the vertical stress was relieved (Figs. 9, 10), the concentration of horizontal stress induced the minor principal stress (which was vertical stress) to be tensile (positive value up to 1.4 MPa). Compressive stress in the upper portion and tensile stress in the lower portion within a hanging rock layer suggested that the main roof strata behaved as voussoir beams [10].

At the two sides of the hanging roof, the stress concentration in the upper and lower portions of the rock layer, however, contrasted with those at the middle (Fig. 12a). At these sides, the undisturbed strata clamped one end of the rock layer. In contrast, the other end moved downwards with the deflection of the voussoir beam. The rock layer at the sides behaved as a cantilever beam whose bending resulted in horizontal stress relief and concentration in its upper and lower portions, respectively. This stress concentration was mentioned earlier in Section 4.1. Figure 12b shows that although the minor principal stress on the two sides was relieved, it was still compressive and would become tensile in the next retreat.

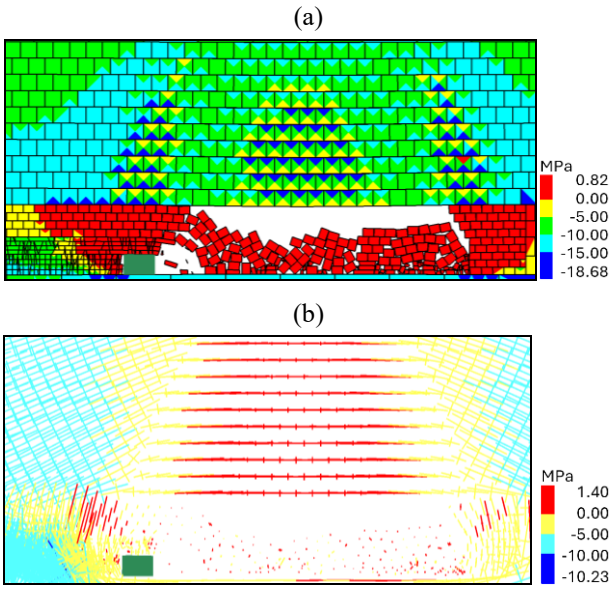

Figure 12. Stress in the roof strata before the first breaking: (a) horizontal stress; (b) minor principal stress

The formation of voussoir beams at the middle and cantilever beams at the two sides of the hanging roof contributed to the verification of the current model.

Once the beam deflection (or sagging) reached its limit, the strata failed and broke at 57 m of retreat for the first time, as shown in Figure 11b. The rocks in the middle and on the two sides mostly failed in tension. The reason was that as the hanging span increased, the tensile stress increased at the locations. When the tensile stress surpassed the tensile strength of the rock, tensile failure occurred. The first weighting was associated with a maximum shield force of 7.16 MN (Fig. 8) and the first breaking of the main roof strata. After this weighting, the shield force dropped to low values of 5-6 MN, and the horizontal stress was relieved through the main roof (Fig. 10c).

The second weighting of roof strata was found to occur at 98 m and was completed at 102 m of retreat modelling. This weighting was associated with a maximum shield force of 7.16 MN (Fig. 8) and the second breaking of the main roof strata (Fig. 11c). Its formation mechanism was as follows. After the first breaking, new cantilever beams in the roof strata were formed. One end of the beam was clamped in the undisturbed strata, while the other rested on and contacted the broken strata. As the mining progressed, the horizontal stress re-concentrated within the beam. It reached a peak magnitude above coal wall (Section 4.1 and Fig. 10d). As explained above, the tensile stress was induced and surpassed the rock tensile strength that resulted in rock tensile failure at the clamped end (Fig. 11c). Apart from the cantilever beam breaking at its clamped end, a secondary breaking near the mid-beam was additionally observed (Fig. 11c). This secondary breaking was likely caused by the beam bending under its deadweight load. The formation and breaking of the cantilever beam were also associated with the following weighting events, where the shield reached its yield force at 114, 126, and 138 m of longwall retreat. It should be noted that before the second weighting, the shield reached a high force of 7.14 MN at 87 m of longwall retreat. Since this force was lower than the yield force and no significant displacement of the roof was recorded, an associated weighting was not formed.

5. Interactions among roof weighting, shield support and coal wall

The interactions among roof weighting, shield support and coal wall were analysed through the parametric studies of key shield and coal characteristics. Using Mine A's longwall model as the basis, each change in a characteristic formed one new model, with other settings being unchanged. The retreat intervals where the first two weighting events occurred and the total number of coal blocks detached from the wall (including its roof) from all retreats were used as interaction indicators. Key characteristics, including shield stiffness, shield setting, yield forces, shield supporting and moving time, coal seam strength, and coal seam stiffness, were changed for the analysis. For the interactions caused by other controlling parameters of weighting, such as panel design and main roof characteristics, the reader is referred to previous studies [18], [34].

5.1. Shield stiffness

Four different values of shield stiffness within the range of 60-160 MN/m were modelled in separate models. This value range represented a practical shield stiffness reported in past studies [5], [22]. The element's displacement for activation of yield force was changed to generate different shield stiffnesses through the models. The results presented in Figure 13 show that when the shield stiffness increased, the first weighting of the main roof occurred consistently at 57-58 m of longwall retreat from its start and corresponded to the first breaking of the main roof strata.

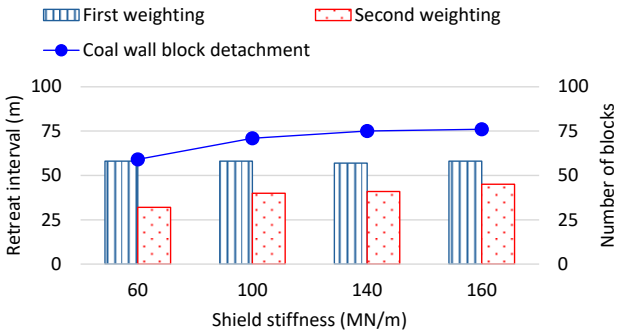

Figure 13. Interaction caused by variation of shield stiffness

The second weighting occurred after the first event at an interval that increased from 32 to 45 m. At the same time, the number of blocks detached from the coal wall has also risen from 59 to 76 blocks. The results indicated that the shield stiffness did not impact its occurrence much for the first weighting because the overburden load was too great. However, for the second weighting, since the stiffer shield better resisted the roof downward displacement under the same loading condition [35], the cantilever roof hung up longer before breaking. The second weighting occurred at a greater interval from the first event. The coal wall should be more stable because a stiffer shield attracts more load. However, the longer span of the cantilever roof transferred more load from itself and overburden strata onto the shield and the coal seam. This consequently caused greater stress concentration and failure in the unmined coal seam. When the coal wall retreated to this area, the failed coal blocks detached more easily from the seam, resulting in more coal wall block detachment, as shown in Figure 13.

5.2. Shield setting force and yield force

The interactions between shield setting force, roof weighting and coal wall were analysed by increasing the set-to-yield ratio within the practical range of 0.6-0.9 [36]. The element's displacement for yield force activation was changed to maintain a constant shield stiffness through all models. The results in Figure 14 show that when the setting force increased, the retreat interval for the first weighting was consistent in the 57-58 m range.

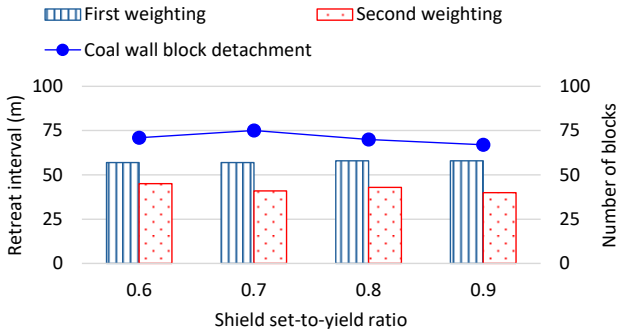

Figure 14. Interaction caused by variation in shield setting force

This weighting was associated with the first breaking of the main roof strata. However, the interval for the second weighting followed a slight decreasing trend from 45 to 40 m. The number of detached coal blocks decreased from 75 to 67 through the models. The results can be explained as follows. The shield setting force did not clearly impact this event for the first weighting because the overburden load was too great. Higher setting forces required a shorter time for the second weighting to reach the first yield event. Within the same cycle time, more yields caused more roof convergence [36]. The roof strata accordingly failed more easily, which shortened the weighting interval. Regarding coal wall detachment, a higher setting force provided extra reinforcement to the immediate roof [37]. This decreased roof delamination and resulted in better coal wall condition. The shorter weighting interval caused better wall conditions, alleviating the stress concentration in the unmined seam, as inferred from Section 5.1. The role of shield setting force in coal wall stability is consistent with that in the literature [37].

Four values of shield yield force within the range of 3.98-10.02 MN were modelled in separate models. This value range represented an industry's practical shield capacity of 811-2044 tons [38]. The setting force and the element's displacement activating yield force were simultaneously changed to maintain a constant shield stiffness through the models.

The results presented in Figure 15 show that when shield capacity increased, the first weighting of the main roof occurred gradually further away from the longwall start, which increased from 55 to 59 m. The event was associated with the first breaking of the main roof strata. Similarly, the second weighting occurred after the first event at an interval that increased from 38 to 43 m.

Note that for the model of great yield force (10.02 MN), the working force was commonly less than the shield yield force through the retreats. The number of detached blocks for the coal wall increased from 63 to 75 before slightly decreesing to 73. The weighting interval and block detachment increased because a higher yield force provided greater resistance to the overburden load.

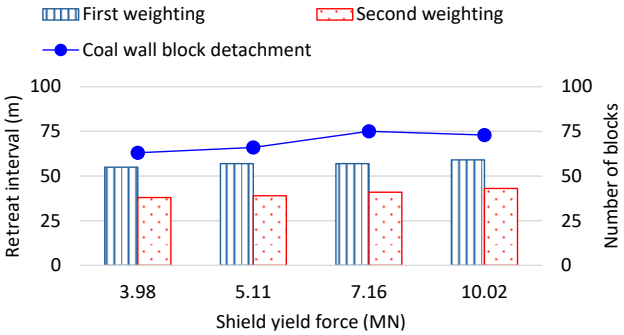

Figure 15. Interaction caused by variation of shield yield force

The shield better resisted roof downward displacement that caused the voussoir and cantilever roof beams to hang for a longer span before breaking. The longer span simultaneously caused greater stress concentration and block detachment. Galvin [5] highlighted that a higher shield capacity can only increase the overhang roof to some extent due to the lever arm effect. Future analysis of shield capacity should combine with ground response as recommended by Barczak and Tadolini [35].

5.3. Shield supporting and moving time

The shield supporting time and moving time greatly control the longwall retreat rate and were therefore changed for interaction analysis. Without a guideline to link the numerical timestep with real time, the numerical timestep for operating the shield in Mine A's model was used as a reference. The timestep for shield supporting mainly varied from 20000 to 150000 steps when a retreat cycle reached equilibrium. For the current analysis, a maximum supporting time limit of 25000-200000 steps per retreat was selected to avoid a longwall retreat too fast or excessive shield loading time.

The results in Figure 16 show that when the supporting time increased, the retreat interval for the first weighting was not impacted. However, the retreat interval for the second event decreased from 48 to 41 m. In contrast, the number of detached coal blocks increased from 66 to 75 blocks. The second weighting interval decreased due to the increasing roof convergence associated with longer shield supporting time. As explained earlier, the shorter weighting interval should lead to less coal wall detachment. However, because the coal wall was exposed for a longer time through the models, more coal wall blocks could complete their detachment, resulting in more coal wall block detachment.

For the shield moving time (also known as shield unsupported time), two extreme cases of immediate shield movement and slow shield movement were analysed apart from the real case of Mine A.

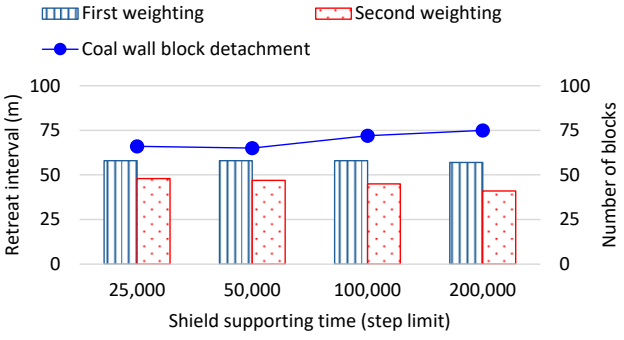

Figure 16. Interaction caused by variation of shield supporting time

The results presented in Figure 17 show that while both first and second weighting intervals decreased, the coal wall detachment increased.

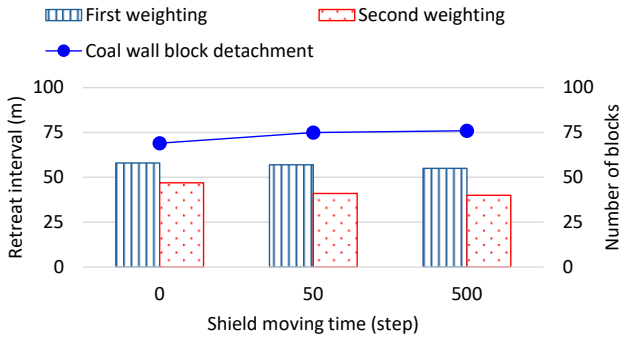

Figure 17. Interaction caused by variation of shield moving time

As explained earlier, the results are consistent with those caused by shield supporting time and can be attributed to the roof convergence and coal wall exposure. All results in Section 5.3 confirm that an increase in longwall retreat rate (decrease in shield supporting and moving time) prolongs the weighting interval, as widely accepted in the literature [39]. To control roof weighting, this retreat rate should be rapid but only to the extent that it remains regular and controlled [5].

5.4. Coal seam strength and stiffness

Four coal cohesion values within the 0.84-2.53 MPa range were modelled to represent different coal seam strengths. The results presented in Figure 18 show that when the seam strength increased, the first weighting occurred gradually away from the longwall start, which increased from 55 to 58 m. The interval where the second weighting happened after the first event also rose from 16 to 41 m in the first three models before decreasing to 36 m in the fourth model. The reason for the increasing trend in the weighting interval was as follows. When the coal strength increased, the coal seam could remain intact for a longer span of roof hanging. The longer span caused greater stress concentration until this stress exceeded the coal's strength. The seam provided more resistance to roof convergence and accordingly delayed the occurrence of roof weighting.

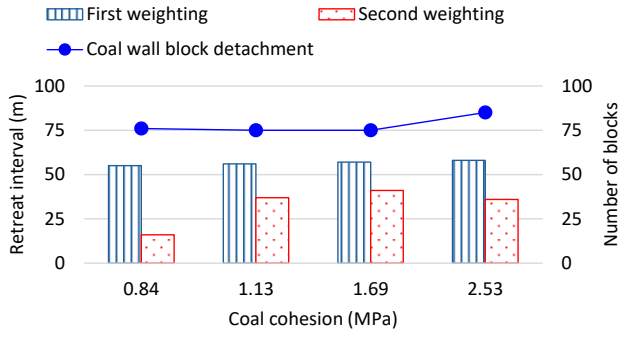

Figure 18. Interaction caused by variation of coal seam strength

Figure 18 also shows that the number of detached coal blocks was consistent in the first three models before increasing to 85 blocks in the last model. There was no clear trend for coal wall detachment because while a stronger seam was more difficult to fail and detach, a longer interval between weighting events caused more stress concentration in the coal seam. Considering both intact coal and in-seam geological structures, a better representation of seam strength is required for future studies.

The coal seam stiffness was analysed by varying the coal elastic modulus in the 0.52-3.09 GPa range. The results presented in Figure 19 show that when the seam stiffness increased, the first weighting of the main roof occurred consistently at 57-58 m of longwall retreat.

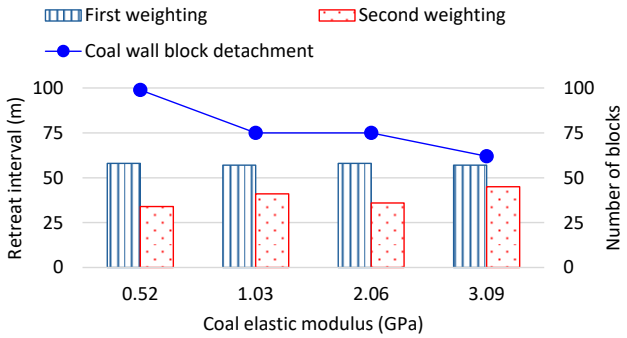

Figure 19. Interaction caused by variation of coal seam stiffness

This result is similar to that caused by shield stiffness and was attributed to the significant overburden load (Section 5.1). The second weighting occurred after the first event at an interval increasing from 34 to 45 m. This trend increased because stiffer coal seams better resisted roof convergence and delayed roof weighting. Figure 19 shows a significant decrease in coal wall detachment from 99 to 62 blocks. Although the longer weighting interval could cause greater stress concentration in the unmined seam (Section 5.1), the stiffer seam increasingly inhibited block deformation and displacement. The coal wall, therefore, became more stable when seam stiffness increased. Better representation of seam stiffness, considering both material property and seam geometry, is recommended for future studies.

6. Discussion and further research

Rock mass surrounding an underground space, especially in the case of longwall mining, may experience severe instabilities if the overburden facilitates a weighting event despite resistance from shield support and coal wall. Using the real-time monitoring data of shield and geological-mining conditions, this paper develops a panel-scale DEM model of longwall retreat to understand the mechanism of mining-induced weighting better. Compared to previous studies [9], [11], [12], this study sufficiently represents first weighting and subsequent events. This is mainly due to the sufficient modelling of total retreat length and web cutting thickness. The mechanism of weighting events is more thoroughly studied by considering simultaneous interactions among roof strata, shield support and coal wall, which has not been entirely performed in previous studies [14]. The interactions are investigated through broad geomechanical behaviours such as:

– stress tensor distribution around underground space;

– stress concentration, stress relief, and rock failure in the main roof strata;

– coal block detachment at the side (wall) and roof (between the wall and shield) of the mining space;

– shield force exerted by roof displacement.

For coal wall, the representation of in-seam fractures as a discrete fracture network, rather than simplified join sets in a previous study [10], leads to a more realistic response

of the wall (e.g., spalling, cavity) to roof weighting. For shield support, because the setting force, yield force and associated leg convergences are modelled based on real shield specifications and ground control curve, the shield sufficiently responds to roof strata displacement. These behaviours of coal wall and shield contribute to more reliably identifying a weighting event.

Within the data range used for the analysis, the findings of this paper provide the reader with a better visualisation of stress distribution and rock mass failure around an underground mining space. This is particularly helpful to engineers in better identifying potential geotechnical hazards that the mining induces. The detailed modelling of this paper should help the reader and engineers develop their model for studying a practical problem. Based on the findings from the interactions among roof weighting, shield support and coal wall, mining engineers can develop technical solutions to improve coal wall and shield stability. This accordingly increases the level of safety at work and maintains the production schedule. Although the findings are helpful for both earth sciences and practice, it should be mentioned that the modelling was two-dimensional in nature. Future studies using a three-dimensional program are recommended to analyze real longwall operations better. In addition, because the shield yield valve was not modelled for model simplification, this valve should be considered in upcoming research better to represent roof convergence and associated coal wall behaviour.

7. Conclusions

This paper provides a detailed understanding of longwall mining-induced weighting from its first occurrence to subsequent events and its interactions with shield support and coal wall. The study confirms that the weighting events are associated with the formation and failure of voussoir beams and cantilever beams within the main roof strata. The study details the profiles of both horizontal and vertical stresses in the main roof strata. During periodic weighting, a re-concentration of horizontal stress at the clamped end of the cantilever roof beam is demonstrated, which reaches a peak of 1.5 times the pre-mining value. Apart from the primary breaking at the clamped end, a cantilever roof beam may experience a secondary breaking near its middle. Within the main roof, the intact rocks were found to fail in tension, while the geological structures mostly failed in shear.

The study reveals that while an increase in shield stiffness and yield force delays the occurrence of the weighting event, the associated longer span of the voussoir/cantilever roof beam increases the coal block detachment at the wall. In contrast, an increase in the set-to-yield ratio of the shield shortens the weighting intervals, and this accordingly decreases the coal wall detachment. For coal seams, both stiffer coal and stronger coal delay the occurrence of weighting. The stiffer coal, meanwhile, clearly improves coal wall stability despite the negative impact from the greater weighting interval. Similarly, a faster longwall retreat rate improves coal wall stability while delaying the weighting occurrence. The findings of this paper, within the data range being analysed, should assist engineers in better identification and response to geotechnical hazards in underground space, maintaining a safe workplace, and minimising environmental impact and resource loss.

Author contributions

Conceptualization: TDL; Formal analysis: TDL, MTT; Methodology: TDL; Writing – original draft: TDL; Writing – review & editing: CKN. All authors have read and agreed to the published version of the manuscript.

Funding

This research is funded by the Vietnam Ministry of Education and Training (MOET) under grant number B2023-MDA-05.

Acknowledgements

Mr. Dan Payne and Mr. Bob Coutts are sincerely acknowledged for their permission to use field data.

Conflicts of interest

The authors declare no conflict of interest.

Data availability statement

The original contributions presented in the study are included in the article, further inquiries can be directed to the corresponding author.

References

[1] Trueman, R., Callan, M., Thomas, R., & Hoyer, D. (2010). Quantifying the impact of cover depth and panel width on longwall shield-strata interactions. *Proceedings of the Coal Operators' Conference*, 97-103.

[2] Commonwealth of Australia. (2014). *Subsidence from coal mining activities*. Canberra, Australia: Australia Government, Department of Environment, 82 p.

[3] Gray, I., & Gibbons, T. (2020). Longwall behaviour in massive strata. *Proceedings of the 2020 Coal Operators' Conference*, 74-103.

[4] Peng, S.S. (2019). *Longwall mining*. London, United Kingdom: CRC Press/Balkema, 562 p. https://doi.org/10.1201/9780429260049

[5] Galvin, J.M. (2016). *Ground engineering – Principles and practices for underground coal mining*. Bern, Switzerland: Springer International Publishing, 684 p. https://doi.org/10.1007/978-3-319-25005-2

[6] Frith, R. (2017). Structural engineering principles in coal mine ground control – The common link between empirical models, numerical models, and practical solutions. *Advances in Coal Mine Ground Control*, 67-92. https://doi.org/10.1016/B978-0-08-101225-3.00004-9

[7] Coutts, R.J., Lynch, D.G., Martin, M.R., & Mills, K.W. (2018). Management of initial convergence events at Broadmeadow mine. *Proceedings of the 37th International Conference on Ground Control in Mining*, 151-160.

[8] Gray, I., & Gibbons, T. (2023). A structural engineering approach to longwall rock mechanics in massive strata. *Proceedings of the 2023 Resource Operators Conference*, 18-35.

[9] Shabanimashcool, M., Jing, L., & Li, C. (2014). Discontinuous modelling of stratum cave-in in a longwall coal mine in the Arctic area. *Geotechnical and Geological Engineering*, *32*(5), 1239-1252. https://doi.org/10.1007/s10706-014-9795-y

[10] Le, T.D., Oh, J., Hebblewhite, B., Zhang, C., & Mitra, R. (2018). A discontinuum modelling approach for investigation of longwall top coal caving mechanisms. *International Journal of Rock Mechanics and Mining Sciences*, *106*, 84-95. https://doi.org/10.1016/j.ijrmms.2018.04.025

[11] Kang, H., Lou, J., Gao, F., Yang, J., & Li, J. (2018). A physical and numerical investigation of sudden massive roof collapse during longwall coal retreat mining. *International Journal of Coal Geology*, *188*, 25-36. https://doi.org/10.1016/j.coal.2018.01.013

[12] Zhou, L., Li, X., Peng, Y., Xia, B., & Fang, L. (2023). Material point method with a strain-softening model to simulate roof strata movement induced by progressive longwall mining. *International Journal of Rock Mechanics and Mining Sciences*, *170*, 105508. https://doi.org/10.1016/j.ijrmms.2023.105508

[13] Gale, W. (2004). Rock fracture, caving and interaction of face supports under different geological environments. Experience from Australian coal mine. *Proceedings of the 23rd International Conference on Ground Control in Mining*, 11-19.

[14] Gao, F., Li, J., Lou, J., Cao, S., & Liu, X. (2021). Understanding the evolution of mining-induced fractures using physical and nu-

merical modeling. *Environmental Earth Sciences*, *81*(1), 22. https://doi.org/10.1007/s12665-021-10141-7
[15] Behera, B., Yadav, A., Singh, G.S.P., & Sharma, S.K. (2020). A numerical modeling approach for evaluation of spalling associated face instability in longwall workings under massive sandstone roof. *Engineering Failure Analysis*, *117*, 104927. https://doi.org/10.1016/j.engfailanal.2020.104927
[16] Murmu, S., & Budi, G. (2022). Analysis of failure associated with longwall face during the main weighting period using a numerical modelling approach. *Mining Technology*, *131*(4), 210-227. https://doi.org/10.1080/25726668.2022.2082152
[17] Wang, J., Wang, Z., & Li, Y. (2020). Longwall top coal caving mechanisms in the fractured thick coal seam. *International Journal of Geomechanics*, *20*(8), 06020017. https://doi.org/10.1061/(ASCE)GM.1943-5622.0001722
[18] Le, T.D., & Bui, X.N. (2020). Effect of key parameters on top coal first caving and roof first weighting in longwall top coal caving: A case study. *International Journal of Geomechanics*, *20*(5), 04020037. https://doi.org/10.1061/(ASCE)GM.1943-5622.0001667
[19] Khanal, M., Adhikary, D., & Balusu, R. (2011). Evaluation of mine scale longwall top coal caving parameters using continuum analysis. *Mining Science and Technology*, *21*(6), 787-796. https://doi.org/10.1016/j.mstc.2011.06.027
[20] Khanal, M., Adhikary, D., & Balusu, R. (2011). Effect of strata properties and panel widths on chock performance. *Journal of Rock Mechanics and Geotechnical Engineering*, *3*, 407-415. https://doi.org/10.3724/SP.J.1235.2011.00407
[21] Singh, G.S.P., & Singh, U.K. (2010). Numerical modeling study of the effect of some critical parameters on caving behavior of strata and support performance in a longwall working. *Rock Mechanics and Rock Engineering*, *43*(4), 475-489. https://doi.org/10.1007/s00603-009-0061-1
[22] Wang, J., Li, M., Wang, Z., Tang, Y., Li, J., Li, Z., & Wang, Z. (2023). A new method for improving coal wall stability in longwall mining by considering support stiffness. *Bulletin of Engineering Geology and the Environment*, *82*(5), 163. https://doi.org/10.1007/s10064-023-03179-3
[23] Gillam, D.J. (2004). *Structural and geomechanical analysis of naturally fractured hydrocarbon provinces of the Bowen and Amadeus basins: Onshore Australia.* Adelaide, Australia: The University of Adelaide, 291 p.
[24] Rajabi, M., Tingay, M., Heidbach, O., Hillis, R., & Reynolds, S. (2017). The present-day stress field of Australia. *Earth-Science Reviews*, *168*, 165-189. https://doi.org/10.1016/j.earscirev.2017.04.003
[25] Xiang, Z., Moon, T., Oh, J., Si, G., & Canbulat, I. (2024). Analytical investigations of in situ stress inversion from borehole breakout geometries. *Journal of Rock Mechanics and Geotechnical Engineering*, *16*(7), 2375-2387. https://doi.org/10.1016/j.jrmge.2023.08.018
[26] Itasca Consulting Group. (2024). *UDEC – Universal Distinct Element Code, Version 7.00.100*. Retrieved from: https://www.itascainternational.com/software/downloads/udec-downloads
[27] Seedsman, R. (1998). *Geotechnical assessment Goonyella exploration adit*. Bowral, Australia: Seedsman Geotechnics Pty Ltd.
[28] Clarkson, L. (2014). *Investigation of shield convergence in underground longwall coal mining, a case study.* Brisbane, Australia: The University of Queensland, 179 p.
[29] Qin, S., Lin, H., Yang, S., & Wei, Z. (2023). A mathematical model for parameter setting in discrete element numerical simulation. *International Journal of Coal Science & Technology*, *10*(1), 87. https://doi.org/10.1007/s40789-023-00644-y
[30] Shen, B., Duan, Y., Luo, X., van de Werken, M., Dlamini, B., Chen, L., Vardar, O., & Canbulat, I. (2020). Monitoring and modelling stress state near major geological structures in an underground coal mine for coal burst assessment. *International Journal of Rock Mechanics and Mining Sciences*, *129*, 104294. https://doi.org/10.1016/j.ijrmms.2020.104294
[31] Bertuzzi, R. (2016). Strength and stiffness properties of defects within the Hawkesbury Sandstone and Ashfield Shale. *Australian Geomechanics Journal*, *51*(3), 95-104.
[32] Seedsman, R. (2021). Assessing the conditions at the boundary of excavations in bedded or foliated rocks. *International Journal of Rock Mechanics and Mining Sciences*, *148*, 104983. https://doi.org/10.1016/j.ijrmms.2021.104983
[33] Mitchell, G.W. (2009). Longwall mining. *Australasian Coal Mining Practice*, 340-375.
[34] Boothukuri, V.R., Bhattacharjee, R.M., Panigrahi, D.C., & Benerjee, G. (2019). Impact of geotechnical factors on strata behavior in longwall panels of Godavari Valley coal field – A case study. *International Journal of Mining Science and Technology*, *29*(2), 335-341. https://doi.org/10.1016/j.ijmst.2018.06.012
[35] Barczak, T.M., & Tadolini, S.C. (2007). Longwall shield and standing gateroad support designs – Is bigger better? *Proceedings of Longwall USA*, 1-26.
[36] Trueman, R., Lyman, G., & Cocker, A. (2009). Longwall roof control through a fundamental understanding of shield–strata interaction. *International Journal of Rock Mechanics and Mining Sciences*, *46*(2), 371-380. https://doi.org/10.1016/j.ijrmms.2008.07.003
[37] Frith, R.C. (2015). A holistic examination of the load rating design of longwall shields after more than half a century of mechanised longwall mining. *International Journal of Mining Science and Technology*, *25*(5), 687-706. https://doi.org/10.1016/j.ijmst.2015.07.001
[38] Wang, J., Zhang, J., & Li, Y. (2015). Ground control in China's coal mine: Progress and prospects. *Proceedings of the 49th U.S. Rock Mechanics/Geomechanics Symposium*, 215-240.
[39] Chen, M., Zhang, C., Canbulat, I., Saydam, S., Fan, G., & Zhang, D. (2024). Assessment of factors and mechanism contributing to groundwater depressurisation due to longwall mining. *International Journal of Coal Science & Technology*, *11*(1), 58. https://doi.org/10.1007/s40789-024-00716-7

Механізм навантаження покрівлі при суцільній системі розробки та його взаємодія з механізованим кріпленням і вугільним масивом

Т.Д. Ле, К.К. Нгуєн, М.Т. Тран

Мета. Дослідження механізму навантаження порід покрівлі, спричиненого вийманням лавами, а також його взаємодії з механізованим кріпленням і вугільним масивом для прогнозування геотехнічної небезпеки у підземному просторі й підвищення безпеки гірничих робіт.

Методика. На основі даних оперативного моніторингу навантажень на механізоване кріплення та гірничо-геологічних умов розроблено панельну чисельну DEM-модель процесу очисного виймання для кращого розуміння геомеханічного механізму навантаження.

Результати. Вивчено розподіли горизонтальних і вертикальних напружень у породах основної покрівлі вугільного пласта. встановлено повторне концентрування горизонтальних напружень біля закріпленого кінця консолі покрівлі під час періодичного навантаження, яке сягає максимуму, що у 1.5 рази перевищує видобувні значення. Визначено, що окрім первинного руйнування біля закріпленого кінця, консоль покрівлі може зазнавати вторинного руйнування поблизу середини прольоту. Встановлено, що у породах основної покрівлі переважає руйнування за розтягом, тоді як геологічні порушення руйнуються переважно за зсувом.

Наукова новизна. Виявлено, що збільшення жорсткості та граничного зусилля спрацьовування механізованого кріплення затримує настання навантаження, однак, водночас призводить до збільшення прольоту консолей, що сприяє відшаруванню вугільного масиву біля вибою. Виявлено, що збільшення співвідношення між початковим і граничним навантаженням кріплення скорочує інтервали між навантаженнями, що, відповідно, зменшує відшарування вугілля на вибої. Більш жорстка та міцна вугільна товща затримує настання навантаження.

Практична значимість. Отримані результати дають змогу краще ідентифікувати геотехнічні загрози в підземному просторі та оперативно реагувати на них, що сприяє підвищенню безпеки робочого середовища та зменшенню негативного впливу на довкілля.

Ключові слова: *підземний видобуток, навантаження покрівлі, руйнування покрівельної балки, моніторинг у реальному часі, конструкція механізованого кріплення, стабільність вугільної стінки*

Publisher's note

All claims expressed in this manuscript are solely those of the authors and do not necessarily represent those of their affiliated organizations, or those of the publisher, the editors and the reviewers.